

α -particle production in the scattering of ${}^6\text{He}$ by ${}^{208}\text{Pb}$ at energies around the Coulomb barrier

D. Escrig^a, A.M. Sánchez-Benítez^{b,c}, A. M. Moro^{d,*},
 M.A.G. Álvarez^d, M.V. Andrés^d, C. Angulo^c, M. J. G. Borge^a,
 J. Cabrera^c, S. Cherubini^e, P. Demaret^c, J.M. Espino^d,
 P. Figuera^e, M. Freer^f, J.E. García-Ramos^b,
 J. Gómez-Camacho^d, M. Gulino^e, O.R. Kakuee^g, I. Martel^b,
 C. Metelko^f, F. Pérez-Bernal^b, J. Rahighi^g, K. Rusek^{b,h},
 D. Smirnovⁱ, O. Tengblad^a, V. Ziman^f

^a*Instituto de Estructura de la Materia, CSIC, E-28006, Madrid, Spain*

^b*Departamento de Física Aplicada, Universidad de Huelva, E-21071, Spain*

^c*Institut de Physique Nucléaire and Centre de Recherches du Cyclotron, Université catholique de Louvain, B-1348 Louvain-la-Neuve, Belgium*

^d*Departamento de Física Atómica, Molecular y Nuclear, Universidad de Sevilla, Apdo. 1065, E-41080 Sevilla, Spain*

^e*INFN Laboratori Nazionali del Sud, I-95123 Catania, Italy*

^f*School of Physics and Astronomy, University of Birmingham, B15 2TT Birmingham, United Kingdom*

^g*Van de Graaff Laboratory, Nuclear Research Centre, AEOI, PO Box 14155-1339, Tehran, Iran*

^h*Department of Nuclear Reactions, Andrzej Soltan Institute for Nuclear Studies, Hoza 69, PL-00681 Warsaw, Poland*

ⁱ*Instituut voor Kern-en Stralingsfysica, University of Leuven, B-3001 Leuven, Belgium.*

Abstract

New experimental data from the scattering of ${}^6\text{He}+{}^{208}\text{Pb}$ at energies around and below the Coulomb barrier are presented. The yield of breakup products coming from projectile fragmentation is dominated by a strong group of α particles. The energy and angular distribution of this group have been analyzed and compared with theoretical calculations. This analysis indicates that the α particles emitted at backward angles in this reaction are mainly due to two-neutron transfer to weakly bound states of the final nucleus.

Key words: Nuclear Reactions, Scattering Theory, Halo Nuclei, Breakup Reactions

1 Introduction

Reactions involving nuclei far from stability at energies around the Coulomb barrier provide an excellent tool to study the novel properties of exotic systems. The increase in intensity of radioactive ion beams achieved along the past two decades has contributed decisively to the improvement of the accuracy of these experiments. One of the exotic nuclei that has received more attention in recent years is the ${}^6\text{He}$. Its interesting Borromean structure, consisting of an α core plus two-weakly bound halo neutrons, and its relatively long half-life (807 ms) makes this nucleus an excellent candidate for this kind of experiments. Reactions induced by ${}^6\text{He}$ on several targets [1,2,3,4,5,6] at energies around the Coulomb barrier exhibit some common features, such as a remarkably large cross section for the production of α particles. This effect is clearly associated with the weak binding of the halo neutrons, that favors the dissociation of the ${}^6\text{He}$ projectile in the nuclear and Coulomb field of the target.

To place our work in the appropriate context, we first review some recent experiments with ${}^6\text{He}$ at Coulomb barrier energies. In the work of Aguilera *et al.* [1] a simultaneous analysis of the elastic and two-neutron removal channels for the ${}^6\text{He}+{}^{209}\text{Bi}$ reaction revealed that, at energies below the Coulomb barrier, the reaction cross section is almost exhausted by the α channel while the complete fusion cross section is very small. In a more recent measurement of the same reaction [2] in which neutron- α coincidences were recorded, the authors concluded that more than half of the α particles produced beyond the grazing angle arise from two-neutron transfer to unbound states of the ${}^{211}\text{Bi}$ residual nucleus. Similar conclusions were achieved in an experiment done by Di Pietro *et al.* [3], where about 80% of the measured α particles coming out from the reaction ${}^6\text{He}+{}^{64}\text{Zn}$ were identified as coming from transfer or breakup. As a further example, we mention the measurements of Navin *et al.* for ${}^6\text{He}+{}^{65}\text{Cu}$ at $E_{\text{lab}} = 19.5$ and 30 MeV [4]. The ${}^{66}\text{Cu}$ yield is largely underestimated by statistical model calculations, suggesting that an important fraction of these products have an origin different from fusion evaporation. The observation of the characteristic γ rays from heavy products (such as ${}^{65}\text{Cu}$) in coincidence with projectile-like particles, confirm that these other processes could be 1n and 2n transfer followed by evaporation.

* Corresponding author

Email address: moro@us.es (A. M. Moro).

Recently, Raabe *et al.* [5], measured fission fragments for the reaction ${}^6\text{He}+{}^{238}\text{U}$ at energies around the fusion barrier. Based upon kinematical considerations, they concluded that the large observed yield for fission below the barrier is entirely due to a direct process, the two-neutron transfer. Their conclusions were supported by calculations performed in the distorted wave Born approximation (DWBA) for the two-neutron transfer to excited states of the ${}^{238}\text{U}$ target.

In this work, we present new data for the breakup of ${}^6\text{He}$ on ${}^{208}\text{Pb}$ at energies around the Coulomb barrier, measured at the CYCLONE RNB facility at the Centre de Recherche du Cyclotron (CRC) of the Université catholique de Louvain (UCL), Louvain-la-Neuve, Belgium. The elastic scattering data from the same reaction has been analysed and presented before [7,8,9]. A comprehensive optical model analysis of these data revealed the existence of a long-range absorption effect, which is a clear indication of the presence of reaction mechanisms that remove flux from the elastic channel at distances well beyond the strong absorption radius. The same effect has been also reported in other reactions induced by ${}^6\text{He}$ [10] and by other weakly bound nuclei, such as ${}^{17}\text{F}+{}^{208}\text{Pb}$ [11]. The inclusion of a dynamic polarization potential (DPP) in the phenomenological projectile-target interaction showed that part of this long-range absorption effect arises from the distortion produced in ${}^6\text{He}$ due to the intense dipole Coulomb interaction [12]. The phenomenological optical model required a very large imaginary diffuseness in order to reproduce the elastic data even after the inclusion of the DPP. Thus, the nuclear interaction contributes also to this long-range absorption.

Given the dominance of the ${}^4\text{He}$ channel in these low energy reactions, it is plausible to suggest that the mechanisms responsible for the production of these fragments are also responsible for the long-range absorption effect. Guided by this motivation, in this work we present an analysis of the two-neutron removal channel measured in the same experiment. In this experiment, the energy and scattering angle of the α particles emitted at backward angles were recorded. The purpose of this work is to understand the reaction mechanisms which are relevant in the collision of ${}^6\text{He}$ on ${}^{208}\text{Pb}$, by examining the angular and energy distributions of the α particles produced in the collision. To do this, for each beam energy, the angular distribution as well as the angle-integrated energy distribution of the α particles have been evaluated and compared with theoretical calculations.

The paper is organized as follows. In section 2 we describe the experimental setup and analysis method, and discuss general features of the measured observables. In section 3, we compare these observables with theoretical calculations performed with the transfer to the continuum method, direct breakup calculations using continuum discretized coupled-channels calculations, and neutron transfer calculations in DWBA. In section 4 we discuss our results

and compare them with previous works. Finally, in section 5 we present the summary and outlook of this work.

2 Experimental setup and analysis procedure

The scattering of a ${}^6\text{He}$ beam on a ${}^{208}\text{Pb}$ target was studied at the radioactive beam facility of the CRC/UCL at Louvain-la-Neuve. The ${}^6\text{He}$ beam was produced by the ${}^7\text{Li}(p,2p){}^6\text{He}$ reaction in a LiF powder target with a graphite container. The atomic beam was ionized in an ECR source, purified by magnetic separation and reaccelerated in the CYCLONE110 cyclotron at the CRC/UCL. This technique provides a highly pure beam, essentially free of contaminants. The only contaminant ever observed in this beam has been reported in the work of Miljanic *et al.* [13] where ${}^4\text{He}^1\text{H}_2^+$ ions were observed as an impurity in a 17 MeV ${}^6\text{He}$ beam with a ratio of intensities of 1:5400. For the angular range covered in the present experiment, the contribution of this impurity turned out to be negligible. The ${}^6\text{He}$ beam was produced at laboratory energies of 14, 16, 18 MeV within the first harmonic of the accelerator with an average intensity of $4\cdot 10^6$ ions per second and at 22 MeV at the lowest limit of the second harmonic with an intensity of $1.5\cdot 10^5$ ions per second. A high intensity ${}^4\text{He}$ beam at laboratory energy of 12 MeV was used for normalization of the elastic cross section.

The elastic data obtained from this experiment are published elsewhere [9]. We briefly review here the main features of the setup. For a more detailed description of the experimental setup we refer to previous publications [7,9]. The size of the ${}^{4,6}\text{He}$ beams were reduced by passing the beam through a set of two collimators of 5 mm and 7 mm diameter with the latter at 400 mm from the target. The targets consisted of self-supporting foils of enriched ${}^{208}\text{Pb}$ (87%) mounted on a movable ladder with a thickness of 0.950 mg/cm^2 for the 12 MeV ${}^4\text{He}$ and 14,16,18 MeV ${}^6\text{He}$ beams and 2.080 mg/cm^2 for the 22 MeV ${}^6\text{He}$ beam. The latter was used to compensate for the low intensity of the beam.

The reaction products were measured using four LEDA detectors in the standard form and six LEDA detectors in the LAMP configuration covering angles in the forward direction from 5° to 65° . For a detailed description of the performance and efficiency of these detectors see [14]. In the backward direction, the most relevant for this analysis, the DINEX telescope array [15,7] was placed at a distance of 37 mm and 42 mm from the 0.950 mg/cm^2 and 2.080 mg/cm^2 thick ${}^{208}\text{Pb}$ targets respectively. The DINEX telescope covered therefore different laboratory angles for the different targets ranging from 136.3° to 166.6° for the thin target and from 131.8° to 164.5° for the thick target of 2.080 mg/cm^2 used only for the 22 MeV ${}^6\text{He}$ beam. The DINEX array consisted of

four quadrants forming a CD [15], each composed of single sided Si strip detectors (ΔE) 40 μm thick with sixteen radial strips stacked in a 500 μm thick single PAD Si-detector. Each strip subtended an angle of about 2° , although this value depends on the scattering angle.

The energy calibration was performed using a triple alpha source for the front single sided Si strip detector of the telescope. The telescope as a whole was calibrated using the elastic scattering peaks of the ^4He and ^6He beams from the ^{208}Pb target at different energies below the Coulomb barrier where the elastic peak at backward angles still has significant statistics. To evaluate the energy losses of the beam and ejectiles in the different media, i.e. target thickness and dead layers of the front and back detectors, a simulation programme developed by R. Raabe [16] and adapted to the geometry of our setup was used. The energy losses of the $^4,6\text{He}$ ions were calculated in tables using SRIM [17] and inserted into the simulation programme. The fact that the interaction region had a finite size, was also taken into account in the simulations.

In order to obtain the energy of the ejectile we first added the signals from the two detectors of the telescope, ΔE and E . The latter was multiplied by a matching constant $\alpha(\theta)$ that depends on the relative gain of the different electronic chains (see [9] for more details). Then we used the energy of the elastic peaks of ^4He at 12 MeV and ^6He at 14, 16 and 18 MeV to calibrate the total telescope signal.

The DINEX telescopes allow mass and charge separation of the reaction products. A typical mass spectrum, ΔE versus total energy, E_T , obtained with the DINEX array for a ^6He beam energy of 22.0(1) MeV and $\theta_{\text{lab}} = 144^\circ \pm 1^\circ$ is shown in Fig. 1. Using these calibrations and the mass and charge separation obtained with the telescopes we are able to identify the energy distribution of the breakup products as well as the elastic counts in every ring (θ_i), as shown in this figure. The energy loss in the 40 μm thick ΔE detector is displayed versus total energy. The ellipsoids select the elastic and breakup events used in the analysis. The low energy selection corresponds to protons. The background events are remarkably low considering that no condition beyond coincidence between the front and back detectors of the telescope is applied.

We obtained the breakup cross section by making use of the ratio of breakup to elastic events seen in the telescopes. To have reasonable statistics, we grouped the breakup events in 1 MeV bins. Then, we evaluated for each detector strip θ_i and for each energy bin E_i the ratio of breakup to elastic events $N_{bu}(\theta_i, E_i)/N_{el}(\theta_i)$. Note that uncertainties associated with beam intensity, solid angle, efficiency of the electronic chain or target thickness disappear in this ratio. When we add these ratios for all the energy bins, we obtain the ratio of breakup to elastic cross sections as a function of the scattering angle. These ratios are shown in Fig. 2, as a function of the laboratory scattering (LAB)

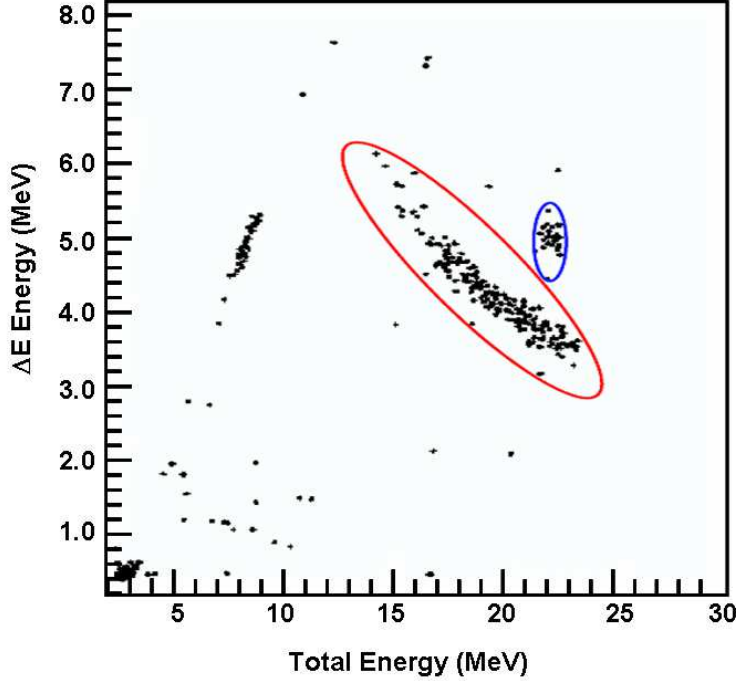


Fig. 1. Two dimensional plot of the 22 MeV ${}^6\text{He}$ scattered from a 2.08 mg/cm^2 ${}^{208}\text{Pb}$ target at laboratory angle of $144(1)^\circ$. The regions enclosed by solid lines correspond to the ${}^6\text{He}$ and ${}^4\text{He}$ events. The plot includes all events in coincidences with multiplicity ≥ 1 to stress the low background level. Therefore one can see events fully stopped in the ΔE detector corresponding to α 's from the grand-daughter of ${}^{210}\text{Pb}$ and ${}^{234}\text{Th}$ present in the target in very small amount. The count rate was less than two α particles every 10 min for this angular coverage.

angle , at several beam energies. It is noticeable that, at $E_{\text{lab}} = 22 \text{ MeV}$, the yield of α fragments exceeds the elastic ones by a factor of ten. As discussed in the introduction, this large α cross section has been reported for other reactions induced by ${}^6\text{He}$ on several medium-heavy targets, such as ${}^{65}\text{Cu}$ [4], ${}^{64}\text{Zn}$ [3], and ${}^{209}\text{Bi}$ [1].

The breakup double differential cross section, with respect to the angle and the energy of the α particle, depends on energy and angle, and can be related to the ratio of the number of counts and to the elastic differential cross section by the following expression:

$$\left. \frac{d^2\sigma_{bu}}{dE d\Omega} \right|_{E_j, \theta_i} = \frac{N_{bu}(\theta_i, E_j)}{N_{el}(\theta_i)} \frac{1}{\Delta E_j} \left(\frac{d\sigma_{el}}{d\Omega} \right)_{\theta_i} \quad (1)$$

where $\Delta E_j = 1 \text{ MeV}$ is the bin width. The differential elastic cross section for the different laboratory angles are taken from [9,18].

If this expression is integrated over the energy of the breakup fragment, one obtains the differential breakup cross section, as a function of the scattering

angle, which is given by:

$$\left. \frac{d\sigma_{bu}}{d\Omega} \right|_{\theta_i} \approx \sum_{j=E_{min}}^{j=E_{max}} \frac{N_{bu}(\theta_i, E_j)}{N_{el}(\theta_i)} \left(\frac{d\sigma_{el}}{d\Omega} \right)_{\theta_i}. \quad (2)$$

These differential cross sections are presented in Fig. 3. Errors bars correspond to statistical errors. It should be noted that the breakup differential cross sections are highest around the Coulomb barrier ($E = 18$ MeV), and they decrease both at lower energies and higher energies. However, for 14 MeV, which is well below the barrier, the breakup cross sections are still sizeable. This indicates that the mechanism producing alpha particles is effective for projectile-target separations as large as 17.3 fm, which corresponds to the distance of closest approach for a head-on collision at this energy. This mechanism, indeed, will be a source of the long range absorption which we have seen in the analysis of elastic data.

Similarly, if, for each energy bin of the α particles, the double differential cross sections are integrated with respect to the angle, over the angular range covered by the CD detectors, one gets a breakup differential cross section as a function of the energy, which is given by

$$\left. \frac{d\sigma_{bu}}{dE} \right|_{E_j} \approx \sum_{i=1}^{i=16} 2\pi \sin(\theta_i) \frac{\Delta\theta_i}{\Delta E_j} \frac{N_{bu}(\theta_i, E_j)}{N_{el}(\theta_i)} \left(\frac{d\sigma_{el}}{d\Omega} \right)_{\theta_i}. \quad (3)$$

These cross sections are presented in Fig. 4.

Our purpose is to understand which mechanism is responsible for the large production of α particles. The fact that the α particles are produced with relatively large energies, that increase with the projectile energy, leads us to conclude that the process should be a direct one, and not a compound nucleus formation. Within the direct mechanism picture, we can consider three mechanisms:

a) Transfer to the continuum: As the ${}^6\text{He}$ nucleus gets close to the target, it leaves the two neutrons with low kinetic energy with respect to the ${}^{208}\text{Pb}$ target, and the remaining α particle escapes. If this is the case, we would expect that the α particle would have an energy distribution centered around the energy of the elastically scattered ${}^6\text{He}$.

b) Direct breakup: The ${}^6\text{He}$ nucleus breaks up in the field of the target and it goes to a continuum state with low excitation energy. In this case, we would expect that the α particle (and the neutrons) to have a similar velocity to the elastically scattered ${}^6\text{He}$, and hence its energy would have a broad distribution around 4/6 of the energy of ${}^6\text{He}$.

c) Neutron transfer: One of the neutrons of ${}^6\text{He}$ is transferred to the target,

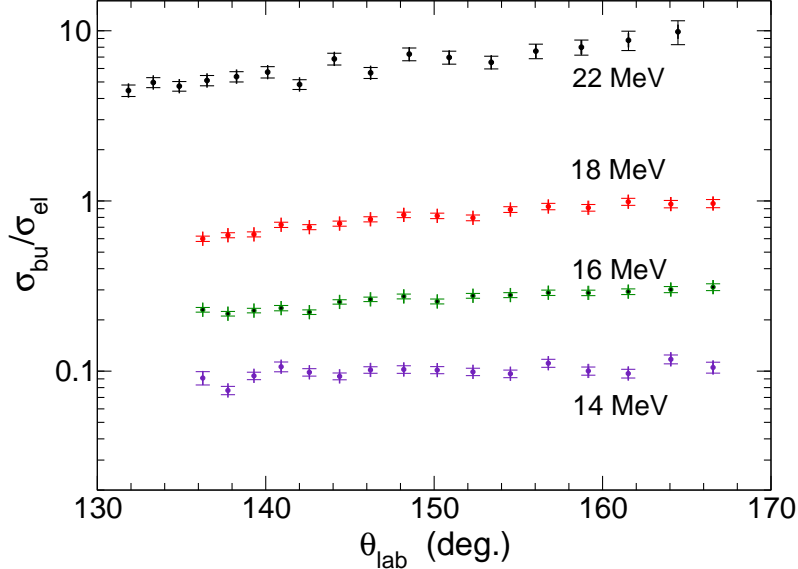


Fig. 2. Ratio between the measured ^4He and ^6He events, as a function of the laboratory scattering angle, at several bombarding energies. The angular range at 22 MeV is different to that covered at energies below the Coulomb barrier due to different positioning of the target. See section 2 for more details. Errors bars correspond to statistical errors.

producing a bound state of ^{209}Pb and leaving ^5He in a broad resonance, that rapidly decays producing ^4He . In this case, the kinetic energy of the ^5He resonance, although dependent on the Q-value, would be similar to that of the elastically scattered ^6He (for $Q \simeq 0$), and the alpha particles would have a broad distribution around 4/5 of the energy of ^5He .

It should be noted that, in our work, direct breakup, 2n transfer and 1n transfer correspond to different approaches to describe the mechanism that produce alpha particles, rather than to different reaction channels. From the theoretical point of view, these three mechanisms describe the removal of the valence neutrons in ^6He , but they do not lead necessarily to different final states. They should be seen as different approaches to a very difficult 4-body problem ($\alpha + n + n + ^{208}\text{Pb}$) which cannot be solved accurately. Each of these methods emphasize a different way in which the fragmentation is produced. In the direct breakup method, one assumes that the ^6He is broken up by exciting the neutrons to continuum states with low relative energy with respect to the α core, and hence a representation in terms of the ^6He continuum states is used. In the transfer to the continuum approach, it is assumed that the fragmentation occurs by transfer of the valence neutrons to weakly bound states of the target, and hence a target representation is preferred in this case. Finally, the 1n transfer corresponds to an intermediate situation, in which one assumes that one of the neutrons is transferred to states of low relative energy with respect to the target, while the other remains in a low energy state with respect to the alpha core. Then, these approaches should be understood as

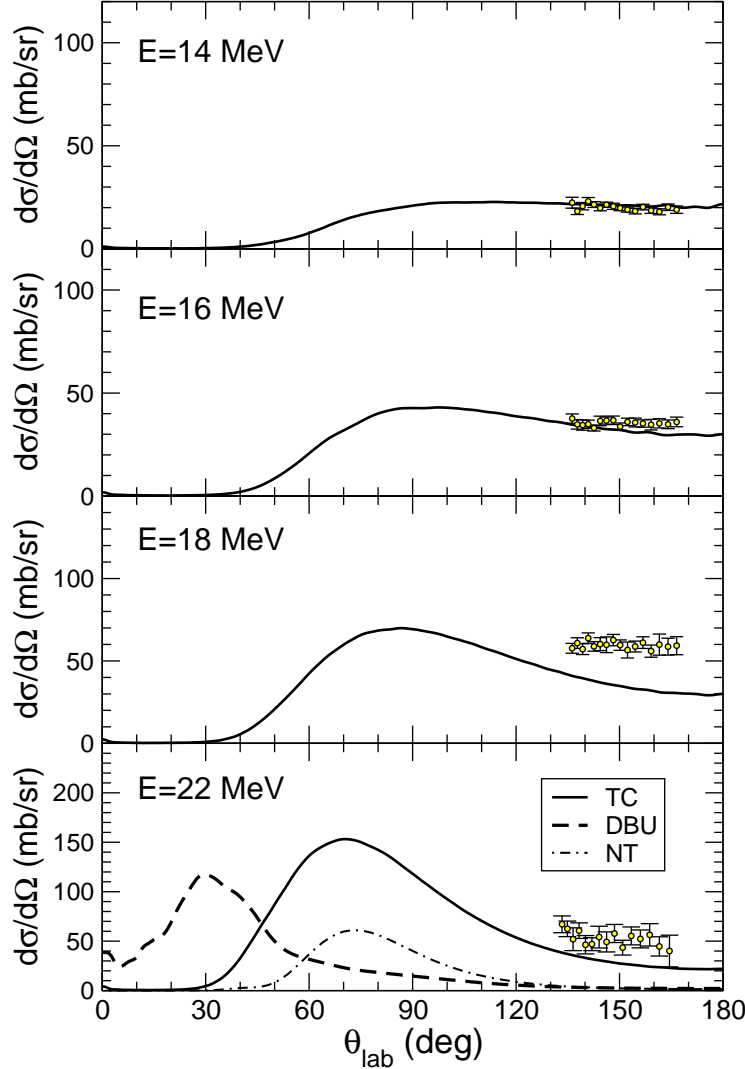


Fig. 3. Angular distribution of α particles arising from ${}^6\text{He}$ fragmentation, in the laboratory frame, for several incident energies. Experimental angular distributions are compared with transfer to the continuum (TC) calculations (solid lines). The distribution obtained at 22 MeV is also compared with a direct breakup (DBU) calculation, performed within the CDCC approach (dashed line), and a DWBA calculation for the one neutron transfer (NT) leading to bound states of the ${}^{209}\text{Pb}$ nucleus (dotted-dashed line).

extreme pictures that emphasize different degrees of freedom of the breakup process, and not different reaction channels. For instance, it has been shown [19] that, if a large basis is included in both the direct breakup and transfer to the continuum representations, there is a strong overlap between the states populated in both methods. As a consequence, the cross sections calculated within the two approaches can not be simply added to obtain the total breakup cross section.

It is apparent from Fig. 4 that the position of the energy peak is not consistent

with the expected value in a direct breakup picture, in which the fragments are produced with essentially the beam velocity. The results for this estimate, calculated at $\theta_{\text{lab}} = 151^\circ$, are shown by the arrows in Fig. 4. Notice that these values are significantly smaller than the measured energy of the α particles and hence it is not expected that the direct breakup model is suitable for understanding the present data.

Under the assumption that the relative energy between the halo neutrons remains small during the process, the gain of kinetic energy of the outgoing α particles implies that these neutrons are left with a small (or even negative, if they are transferred to bound states) relative energy with respect to the target. Energy conservation demands that the available kinetic energy is used to excite the target, or to accelerate the α particles, as we observe in this experiment. This indicates that the processes responsible for the production of these α fragments are of a more complicated nature than suggested by the simple direct breakup model.

From these semiquantitative considerations, our data suggest a transfer to the continuum picture, in which the valence neutrons are transferred to highly excited states of the target, lying around the $^{210}\text{Pb} \rightarrow ^{208}\text{Pb} + 2\text{n}$ breakup threshold. Final states above this threshold can be interpreted as a three-body breakup of the projectile, while those below the threshold would correspond to a pure transfer process leading to bound states of the ^{210}Pb residual nucleus.

3 Theoretical calculations

In this section, we present a more quantitative analysis of the data, by performing calculations for the different mechanisms described in the preceding section (transfer to the continuum, direct breakup or one neutron transfer). The goal of this study is to see which of these mechanisms is more appropriate to describe the present data.

3.1 *Transfer to the continuum*

We use the transfer to the continuum method, in which the two-neutron removal is treated as a transfer of the valence neutrons to bound and unbound states of the $2\text{n} + ^{208}\text{Pb}$ system. For simplicity, these calculations are performed within the DWBA approximation. Although the DWBA method has been traditionally applied to the transfer between bound states, it has also proved to be a useful method in situations where final states lie in the continuum [20,21,22,23,24]. To simplify our description of the reaction process, we assume

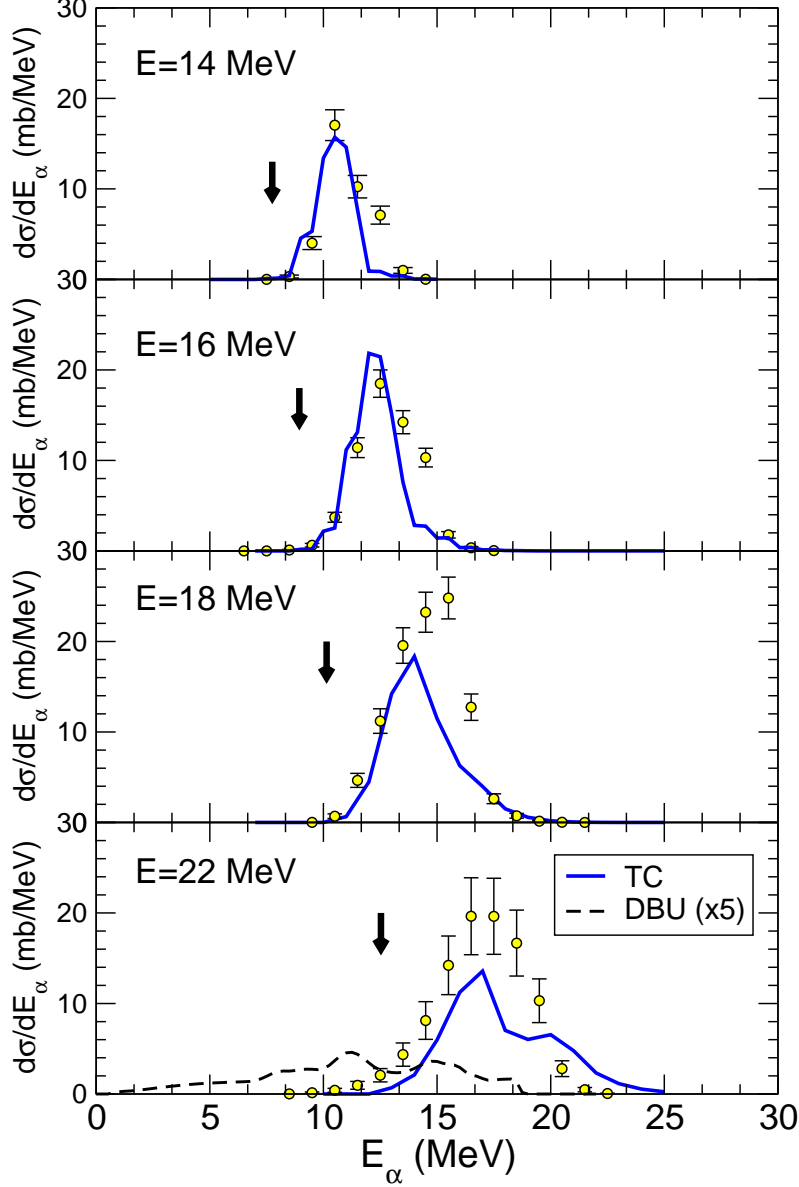


Fig. 4. Energy distribution of detected α particles for the reaction ${}^6\text{He}+{}^{208}\text{Pb}$ at 14, 16, 18 and 22 MeV, integrated in the angular range 132° - 164° . Experimental data (circles) are compared with transfer to the continuum (TC) calculations (solid lines). The arrows indicate the expected energy of the α particles scattered at $\theta_{\text{lab}} = 151^\circ$, assuming an extreme direct breakup picture. In the panel for $E_{\text{lab}} = 22$ MeV the full direct breakup calculation, performed within the CDCC method, is also presented, multiplied by a factor of 5.

that the relative motion of the two halo neutrons is not affected during the process. At least for the Coulomb interaction, which is known to be very important in this reaction, this assumption is expected to be reasonable because this interaction will act only on the α fragment, tending to stretch the ${}^6\text{He}$ system, with the neutrons moving against the α core. So, in these calculations, we emphasize the dineutron- α relative coordinate, under the assumption that

this is the ${}^6\text{He}$ main degree of freedom which is excited during the process. These transfer couplings are schematically depicted in Fig. 5a.

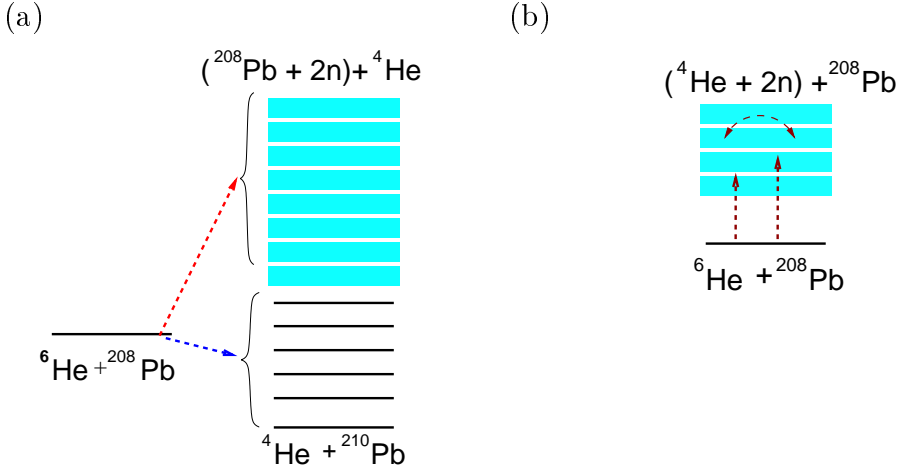


Fig. 5. Schematic representation of the couplings included in the transfer to the continuum (a) and direct breakup (b) calculations.

In this reaction, the post form expression of the DWBA transition amplitude involves a matrix element of the operator

$$V_{[2n-\alpha]} + U_{[\alpha-{}^{208}\text{Pb}]} - U_{[\alpha-{}^{210}\text{Pb}]}.$$

The potential parameters required in the calculations are summarized in Table 1. For the α - ${}^{208}\text{Pb}$ system, we used the parameterization of Barnett and Lilley [25]. The optical potential for the ${}^6\text{He}$ - ${}^{208}\text{Pb}$ system, which is used to generate the distorted waves for the incoming channel, is taken from a fit of the elastic angular distribution [9,18]. The same parameters were used for the outgoing channel (α - ${}^{210}\text{Pb}$). As explained above, the neutron pair was allowed to be transferred to both bound and unbound states of ${}^{210}\text{Pb}$. The $2n$ - ${}^{208}\text{Pb}$ relative wavefunctions were generated with the deuteron- ${}^{208}\text{Pb}$ optical potential derived in Ref. [26]. In order to permit the inclusion of bound states, only the real part of this potential was considered. Reduced radii (r_x) were converted to physical radii (R_x) as $R_x = r_x(A_1^{1/3} + A_2^{1/3})$, for the ${}^6\text{He}$ - ${}^{208}\text{Pb}$ and α - ${}^{210}\text{Pb}$ systems, and as $R_x = r_x$ for the $2n$ - α system.

In the di-neutron model, the ${}^{208}\text{Pb}+2n$ final states should be considered as *doorway states* to which the di-neutron is transferred. The *doorway states* subsequently fragment into bound or continuum states of ${}^{210}\text{Pb}$. To evaluate the wavefunctions of these *doorway states*, we take into account the average separation energy of the $2n$ single particle configurations for each L value, $\langle\epsilon_{2n}\rangle$, according to the available experimental information [28]. Then, we evaluate the number of nodes of the ${}^{208}\text{Pb}$ - $2n$ relative wavefunction, N , preserving the Pauli principle. This is done using the Wildermuth condition [29,30]:

Table 1
Potential parameters used in the calculations.

System	V_0 (MeV)	r_0 (fm)	a_0 (fm)	W_0 (MeV)	r_i (fm)	a_i (fm)	Ref.
${}^6\text{He}-{}^{208}\text{Pb}^a$	b	1.015	1.15	c	1.015	1.70	[9]
$\alpha-{}^{208}\text{Pb}$	96.44	1.376	0.625	32	1.216	0.42	[25]
$2\text{n}-{}^{208}\text{Pb}$	85.55	1.20	0.751	-	-	-	[26]
$2\text{n}-\alpha$	87.18	1.90	0.39	-	-	-	[27]

^a The same parameters were used for the ${}^4\text{He}-{}^{210}\text{Pb}$ distorted potential.

^b $V_0 = 32.8, 31.4, 33.1$ and 5.89 MeV for $E_{\text{lab}} = 14, 16, 18$ and 22 MeV, respectively.

^c $W_0 = 0.04, 4.6, 5.1$ and 9.84 for $E_{\text{lab}} = 14, 16, 18$ and 22 MeV, respectively.

Table 2

$2\text{n}-{}^{208}\text{Pb}$ potentials used to generate the bound and unbound states of the ${}^{210}\text{Pb}$ nucleus in the transfer to the continuum calculations.

J^π	0^+	1^-	2^+	3^-	4^+	5^-	6^+
V_0 (MeV)	85.9	73.2	85.6	100.3	85.6	97.3	85.1
N	7	7	6	6	5	5	4
$\langle\epsilon_{2\text{n}}\rangle$ (MeV)	-4.9	1.0	-4.8	-6.4	-5.0	-5.1	-5.4

$2(N-1) + L = 2(n_1-1) + l_1 + 2(n_2-1) + l_2$, where (n_1, l_1) and (n_2, l_2) are the single-particle configurations which have to be populated in a simple shell model picture to produce a state with the desired J . In all cases, we used a Woods-Saxon form, with radius $1.2 \times 208^{1/3}$ fm and diffuseness $a = 0.75$ fm [26]. Finally, we adjust the potential depth, V_0 , to produce a state with the given L , N , and $\langle\epsilon_{2\text{n}}\rangle$. The case $L = 1$ deserves a special consideration, since no single-particle pair configuration of bound single-particle states couples to $J = 1^-$. To obtain these states one neutron has to be promoted to the next shell, and this will increase the energy of the 1^- state by $\hbar\omega \simeq 6$ MeV, leading to a resonance around $\langle\epsilon_{2\text{n}}\rangle = 1$ MeV, above the two-neutron breakup threshold. Then, the potential depth was adjusted in this case to obtain a resonance at this energy. The values of N , V_0 and $\langle\epsilon_{2\text{n}}\rangle$ are listed in Table 2.

The states of ${}^{210}\text{Pb}$ above the ${}^{208}\text{Pb}+2\text{n}$ threshold are described by means of 1 MeV continuum bins, obtained by superposition of the $2\text{n}-{}^{208}\text{Pb}$ scattering wavefunctions, up to a maximum excitation energy of 8 MeV. Thus, the two-body spectroscopic strength is naturally distributed along the continuum. However, for bound states, the fragmentation does not appear. To take this into account, we consider that the *doorway states* are fragmented into N_b states, with two neutron separation energies of $S_{2\text{n}} = 0.5, 1.5, \dots, 7.5$ MeV, each one with an spectroscopic factor of $1/N_b$. In practice, we took $N_b = 8$ but

we verified that the results did not depend strongly on this number. For the continuum states, we assumed unit spectroscopic factors.

The α -2n interaction, required to generate the ${}^6\text{He}$ ground state wavefunction, was parameterized using a standard Woods-Saxon form, with radius $R_0 = 1.90$ fm and diffuseness $a_i = 0.39$ fm, which corresponds to the set II of Ref. [27]. A pure $2S$ configuration, with unit spectroscopic factor, was assumed for this state. The potential depth was obtained using the energy separation method, that is, the depth was adjusted in order to reproduce the two-neutron separation energy. However, instead of using the experimental separation energy ($S_{2n} = 0.975$ MeV) we used the modified value $S_{2n} = 1.5$ MeV. This change is motivated by the fact that the 2n- α wavefunction, calculated with the experimental separation energy, extends too much in configuration space, as compared to a realistic three-body calculation. As a consequence, couplings to the continuum are largely overestimated, leading to unrealistic results for the scattering observables, as shown recently for the elastic scattering of ${}^6\text{He}+{}^{208}\text{Pb}$ [31] and ${}^6\text{He}+{}^{209}\text{Bi}$ [32]. By increasing the binding energy to $S_{2n} = 1.5$ MeV the wavefunction obtained in the di-neutron model simulates fairly well the three-body wavefunction in the (nn)- α coordinate. The physical idea behind this choice is that, in ${}^6\text{He}$, the neutron-neutron pair contributes to the binding energy with a positive average energy which, added to the (negative) relative energy associated to the (nn)- α motion, should give the correct binding energy. Further details of this method will be published elsewhere [33].

In order to get convergence of the angular cross section within the angular range covered by the present data, we found it necessary to include partial waves up to $L = 6$ for the 2n- ${}^{208}\text{Pb}$ motion. The total angular momentum was set to $J = 50$, and the distorted waves were calculated up to 200 fm. A range of non-locality of 9 fm was required for the transfer couplings. These calculations were performed with the coupled-channels computer code FRESKO [34].

The differential angular distribution for each final state is proportional to the square of the DWBA amplitude. By energy conservation, the energy of the outgoing α particles is obtained from the excitation energy of ${}^{210}\text{Pb}$. This procedure provides a double differential cross section with respect to the angle and energy of the scattered α fragments. In order to permit a meaningful comparison with the data, these magnitudes were transformed to the LAB frame. For this purpose, the calculated center-of-mass (CM) double-differential cross sections were converted to LAB system using the appropriate Jacobian for the kinematical transformation for $(\theta_{\text{c.m.}}, E_{\alpha}^{\text{c.m.}}) \rightarrow (\theta_{\text{lab}}, E_{\alpha}^{\text{lab}})$.

The calculated angular distributions are represented by the solid lines in Fig. 3. The overall agreement with the data is good, although for the higher scattering energies ($E_{\text{lab}} = 18$ and 22 MeV) the experimental distributions are somewhat underpredicted. This underestimation, which could be due to the approxima-

tions involved in our method, might indicate the presence of other channels not included in our calculations. Dynamical effects, such as multi-step transfer processes, not considered in the DWBA calculations, could also affect the results. We would like to note that the calculation of absolute cross sections in two-neutron transfer reactions is a very complicated problem [35,36], and discrepancies as large as one or two orders of magnitude between theory and experiment have been reported by some authors. Keeping in mind these difficulties, the degree of agreement between the present data and the transfer to the continuum calculations is very encouraging.

Finally, the calculated energy distributions of the α particles, in the LAB frame, are given by the solid lines in Fig. 4. The transfer to the continuum calculations (thick solid lines) reproduce very well the shape of these distributions. In particular, the position of the peak is very well accounted for at all energies. The absolute values of these distributions are also reasonably reproduced, except for the underestimation at the higher energies discussed above.

We would like to stress that these calculations do not include any free parameter. They are based on a direct application of a fully quantum mechanical expression of the transition amplitude, within the DWBA approximation, and the ingredients are the potentials between the fragments taken from the literature, and a physically motivated model for the initial and final states in the ${}^6\text{He}$ and ${}^{210}\text{Pb}$ nuclei, respectively.

3.2 *Direct breakup*

The direct breakup component of the α inclusive spectrum could be also calculated within the standard continuum discretized coupled-channels (CDCC) method [37]. In the direct breakup picture, the fragmentation process is formally treated as an inelastic excitation of the projectile to the continuum (see Fig. 5b). From the semiquantitative arguments outlined in Sec. 2, we do not expect this scheme to be appropriate for the present reaction, since the observed energy of the α particles is significantly larger than the values estimated by kinematic considerations assuming a direct breakup picture. These considerations, along with the calculations presented in Sec. 3.1, clearly suggest that the energies of the observed α particles at backward angles are consistent with the transfer of the valence neutrons to weakly bound states of the target. These states are indeed better described in a basis of the target representation, as we have done in the transfer to the continuum calculations. The direct breakup representation, by contrast, is expected to be less efficient in this case, in the sense that a large basis would be required to describe 2n-target states with small relative energy and angular momentum. In order to test these arguments

we have performed CDCC calculations for the $E_{\text{lab}} = 22$ MeV case.

Again, we assumed a simple di-neutron model for ${}^6\text{He}$. Partial waves s , p and d were included for the $2n$ - ${}^4\text{He}$ relative motion. For each partial wave, the ${}^6\text{He}$ continuum was divided into energy bins, according to the scheme detailed in [31]. In analogy with the prescription used in the transfer to the continuum calculations, the effective two-neutron separation energy $S_{2n} = 1.5$ MeV was used to generate the ${}^6\text{He}$ ground state and continuum wavefunctions. With this prescription, the elastic angular distribution is very well reproduced. The breakup angular and energy distributions obtained from this calculation are represented in Figs. 3 and 4 by the dashed line (bottom panel). It can be seen that the experimental data are underestimated by almost an order of magnitude, at all the measured angles. The inclusion of higher partial waves did not solve the discrepancy. Hence, as we anticipated, the direct breakup picture is inadequate to describe the present data. From the figure, we see also that the CDCC distribution dominates the small angle region, with a pronounced peak around 30° . At these angles, the transfer to the continuum curve is very small, suggesting that for the description of the α particles emitted at forward angles the direct breakup scheme should provide a more suitable representation than the TC.

We note that a proper CDCC calculation for the present reaction would require a three-body description of ${}^6\text{He}$, thus giving rise to a four-body scattering problem. This kind of calculations has been recently reported by the Kyushu group for ${}^{12}\text{C}$ [38] and ${}^{209}\text{Bi}$ [32] targets. Although our results will be modified to some extent if a realistic three-body description of ${}^6\text{He}$ is used, we believe that our simplified calculations retain the essential physics to illustrate the inadequacy of the CDCC method to describe the present data.

3.3 One neutron transfer

Another channel that could contribute to the production of α particles is the one neutron stripping, ${}^{208}\text{Pb}({}^6\text{He}, {}^5\text{He}){}^{209}\text{Pb}$. This process will produce ${}^5\text{He}$ in a resonant state, which will eventually decay into $n+{}^4\text{He}$. The calculations for this process were performed within the DWBA approximation. Due to Q -value considerations, this process populates mainly bound states of the ${}^{209}\text{Pb}$ nucleus, similar to what occurs in the ${}^{208}\text{Pb}(d,p){}^{209}\text{Pb}$ reaction [39]. Thus, we included the known bound states for the ${}^{209}\text{Pb}$ nucleus, and assumed unit spectroscopic factors, since these are known to be mainly single-particle states. Concerning the spectroscopic factor for ${}^6\text{He} \rightarrow {}^5\text{He}+n$, in a strict shell model picture, with maximal pairing, spectroscopic factor for neutron transfer is equal to number of valence neutrons, what would give 2. We adopt however the value 1.60 for this spectroscopic factor, reported by Nemets *et al* [40], and

obtained using the method detailed in Ref. [41].

For the entrance channel, ${}^6\text{He}+{}^{208}\text{Pb}$, the effective potential obtained from CDCC calculations was used. For the exit channel, ${}^5\text{He}+{}^{209}\text{Pb}$, the potential was calculated by folding the $n+{}^{209}\text{Pb}$ potential from the compilation of Varner *et al.* [42] and the $\alpha + {}^{208}\text{Pb}$ potential of Goldring *et al.* [43] with the ground state wave function of ${}^5\text{He}$. The latter was represented by an energy bin of a width 1.2 MeV placed at an excitation energy of 0.8 MeV above the ${}^5\text{He}\rightarrow{}^4\text{He}+n$ breakup threshold. The binding potential for ${}^4\text{He}+n$ was taken from Ref. [44].

The calculated angular distribution is shown by the dotted-dashed line in the lowest panel of Fig. 3 ($E_{\text{lab}}=22$ MeV). It should be noted that, in this case, the scattering angle corresponds to the center of mass of the ${}^5\text{He}^*$ system, rather than the ${}^4\text{He}$ angle. At intermediate angles ($\theta_{\text{lab}} \approx 90^\circ$), our calculation predicts a significant contribution of the 1n transfer, although the α yield is still dominated by the 2n transfer. This result is in agreement with the experimental data of De Young *et al.* [2] in which the 2n transfer was identified as the main mechanism producing α particles at these angles, with a small contribution arising from 1n transfer. We note however that the cross sections reported in [2] for the 1n and 2n transfer processes are inferred from the α particles observed at 90 and 120 degrees, while in our experiment the observed α particles correspond to larger angles (above 130°). Therefore, the cross sections reported in Ref. [2] cannot be readily extrapolated to our case. Moreover, even if we compare the same angular range, we do not expect to get the same quantitative results, because the states populated in both reactions (namely, ${}^{209}\text{Pb}$ and ${}^{210}\text{Bi}$) are different.

It can also be seen that at the angles of interest of our experiment ($\theta_{\text{lab}} > 130^\circ$), the contribution of the 1n transfer is negligible and the production of α particles is essentially due to 2n transfer. Moreover, the 1n transfer cannot explain the energy of the α particles since the maximum kinetic energy of the α particles emitted in this process, which corresponds to a transfer to the ${}^{209}\text{Pb}$ ground state, is about 17.5 MeV, while the experimental energy distribution extends beyond 20 MeV. Therefore, we conclude that the one neutron stripping channel is not responsible for the underestimation of the data at these angles.

4 Discussion

The results found in this work are consistent and complementary to our previous analysis of the elastic scattering for the same reaction [9]. The optical model analysis performed in the previous work revealed the importance of a long range absorption mechanism. With the present analysis, one can conclude

that this mechanism is presumably related to the two-neutron removal process discussed in this work. In order to draw more definite conclusions it would be desirable to obtain data in a wider angular range.

Furthermore, in order to understand more clearly the importance of different reaction mechanisms, it would be very useful to perform a similar experiment in which the neutrons could be detected in coincidence with the α particles. Given the small detection efficiency for neutrons, and the fact that the two neutrons can be emitted, in principle, in arbitrary directions, this experiment is also very challenging from the experimental as well as from the theoretical points of view. Despite these difficulties, a similar experiment has been recently performed for the reaction ${}^6\text{He}+{}^{209}\text{Bi}$ at 22 MeV [2]. By measuring neutron- α coincidences it is concluded that approximately 55% of the observed α yield around and beyond the grazing angle is due to two-neutron transfer to unbound states of the ${}^{211}\text{Bi}$ nucleus.

Our results are also consistent with other experiments on ${}^6\text{He}$ induced reactions on several targets, such as ${}^{64}\text{Zn}$ [3], ${}^{65}\text{Cu}$ [4] and ${}^{238}\text{U}$ [5], for which large 1n and 2n transfer cross sections have been inferred using different experimental techniques.

In the case of the reaction using the ${}^{238}\text{U}$ target, these conclusions are supported by the recent calculations of Cárdenas *et al.* [45]. Using a schematic coupled-channels calculations, the authors show that the 2n removal cross section from ${}^6\text{He}$ can be well accounted for by an incoherent superposition of several transfer processes with different Q values. Similarly, the calculations in this work involve also an incoherent sum of 2n transfer to final states with a wide range of Q values.

5 Summary and outlook

In this paper we have presented new experimental data for the reaction ${}^6\text{He}+{}^{208}\text{Pb}$ at energies around and below the Coulomb barrier. The reaction cross section at backward angles is dominated by a prominent ${}^4\text{He}$ group, which was interpreted as coming from projectile fragmentation.

For each scattering energy, the angular and energy distributions of the ${}^4\text{He}$ fragments have been analyzed and compared with transfer to the continuum calculations, in which the two-neutrons are assumed to be transferred as a cluster to both bound as well as unbound states of the target nucleus. According to these calculations, most of the observed α yield comes from the transfer of the valence neutrons to highly excited states of the target in the proximity of the two-neutron breakup threshold. By contrast, direct breakup

calculations and one neutron transfer calculations fail to explain the present data.

This analysis suggests a scenario in which the ${}^6\text{He}$ nucleus is broken up in the field of the target, and the valence neutrons are left with a small relative energy with respect to the target. By energy conservation, the kinetic energy lost by the neutrons is transferred to the α particles, which are therefore accelerated with respect to the beam velocity. These conclusions are consistent with previous measurements for other reactions induced by ${}^6\text{He}$ on several targets, for which large transfer cross section have been also reported [1,2,3,4,5].

Further measurements for this reaction, including complete kinematics, wider angular coverage, detection of fission and evaporation products, etc, would be very useful to disentangle more clearly the importance of different reaction mechanisms, and improve our understanding of the processes that take place in the scattering of exotic nuclei at energies around the Coulomb barrier. Some of these measurements have been already performed and the subsequent analysis is underway.

Despite the reasonable quantitative agreement with the data, the transfer to the continuum calculations can be improved in both the structure and reaction aspects. Concerning the structure model, the main approximation involved in our calculation is the assumption of the validity of the di-neutron model. Four-body DWBA calculations have been performed by Chatterjee *et al.* [46] for the scattering of ${}^6\text{He}$ on Pb and Au at high energies, using a realistic three-body description of the ${}^6\text{He}$ nucleus. By comparing with a conventional three-body DWBA calculation based upon a di-neutron model of ${}^6\text{He}$, they find that the latter calculation gives too large breakup cross section. The disagreement is attributed to the bigger rms radius in the di-neutron model, as compared to a realistic three-body model. In our calculations this effect is accounted for by increasing the 2n separation energy in ${}^6\text{He}$. Also, the description of the final states in ${}^{210}\text{Pb}$ could be improved by using a more realistic level density for this nucleus.

Concerning the description of the reaction mechanism, these calculations could be improved by including couplings among final states in ${}^{210}\text{Pb}$, by means of the CCBA method. These couplings could be generated in a cluster model, by folding the 2n- α and α - ${}^{208}\text{Pb}$ interactions with the internal wavefunctions for the ${}^{210}\text{Pb}$ states. Also, couplings between the transfer/breakup channels and the elastic channel could be incorporated beyond the first order, thus performing a coupled-reaction channels calculation. This calculation would permit an assessment of whether the explicit inclusion of these channels can explain the long-range absorption effect encountered in the analysis of the elastic data. If this is the case, the optical potential required to reproduce the elastic data in presence of transfer channels should have a smaller

diffuseness, as compared to the phenomenological optical potential derived in absence of these channels. Notice that, in the DWBA approach, these higher order effects are accounted for in an effective way by an appropriate choice of the phenomenological optical potentials used to describe the incoming and outgoing distorted waves. These CCBA and coupled reaction channels calculations are beyond the scope of this work, and hence they have not been attempted.

Acknowledgements

This work has been supported by the Spanish MCyT projects FPA2005-04460, FPA2005-02379, FPA-2000-1592-C03-02, FPA2003-05958, and FPA2002-04181-C04-02/03, by the European Community-Access to Research Infrastructure action of the Improving Human Potential Program, contract number HPRI-CT-1999-00110 and the Belgian program P5/07 on interuniversity attraction poles of the Belgian-state Federal Services for Scientific, Technical and Cultural Affairs. We are grateful to J. Kolata for useful discussions. A.M.M. acknowledges financial support by the Junta de Andalucía. D.E. acknowledges financial support by the MEC.

References

- [1] E. F. Aguilera *et al.*, Phys. Rev. Lett. 84 (2000) 5058–5061.
- [2] P. A. DeYoung *et al.*, Phys. Rev. C71 (2005) 051601.
- [3] A. Di Pietro *et al.*, Phys. Rev. C 69 (2004) 044613.
- [4] A. Navin, *et al.*, Phys. Rev. C 70 (2004) 044601.
- [5] R. Raabe, *et al.*, Nature (London) 431 (2004) 823.
- [6] J. F. Liang, C. Signorini, International Journal of Modern Physics E (2005) 1121–1150.
- [7] A. M. Sánchez-Benítez, *et al.*, J. Phys. (London) G31 (2005) S1953.
- [8] O. R. Kakuee, *et al.*, Nucl. Phys. A765 (2006) 294.
- [9] A. M. Sánchez-Benítez *et al.*, Submitted to Nuclear Physics A.
- [10] E. F. Aguilera *et al.*, Phys. Rev. C 63 (2001) 061603.
- [11] A. Romoli *et al.*, Phys. Rev. C 69 (2004) 064614.

- [12] M. V. Andrés, J. Gómez-Camacho, M. A. Nagarajan, Nucl. Phys. A 579 (1994) 273.
- [13] D. Miljanic et al., Nucl. Inst. and Methods 447 (2000) 544–547.
- [14] T. Davidson et al., Nucl. Instrum. Methods A 454 (2000) 350.
- [15] A. N. Ostrowski, S. Cherubini, T. Davinson, D. Groombridge, A. M. Laird, A. Musumarra, A. Ninane, A. di Pietro, A. C. Shotter, P. J. Woods, Nucl. Inst. and Methods 480 (2002) 448.
- [16] R. Raabe, Ph. D. Thesis, Katholieke Universiteit Leuven, Belgium.
- [17] SRIM code can be downloaded at <http://www.srim.org>.
- [18] A. M. Sánchez-Benítez, Ph.D. Thesis. University of Huelva. Unpublished.
- [19] A. M. Moro, F. M. Nunes, Nucl. Phys. A 767 (2006) 138.
- [20] C. M. Vincent, H. T. Fortune, Phys. Rev. C 2 (1970) 782.
- [21] H. Frohlich, T. Shimoda, M. Ishihara, K. Nagatani, T. Udagawa, T. Tamura, Phys. Rev. Lett. 42 (1979) 1518.
- [22] G. Baur, D. Trautmann, Phys. Rep. 25 (1976) 293.
- [23] T. Udagawa, Y. Lee, T. Tamura, Phys.Rev. C 39 (1989) 47.
- [24] A. M. Moro, R. Crespo, H. García-Martínez, E. F. Aguilera, E. Martínez-Quiroz, J. Gómez-Camacho, F. M. Nunes, Phys. Rev. C 68 (2003) 034614.
- [25] A. R. Barnett, J. S. Lilley, Phys. Rev. C 9 (1974) 2010.
- [26] W. W. Daehnick, J. D. Childs, Z. Vrcelj, Phys. Rev. C 21 (1980) 2253.
- [27] K. Rusek, K. W. Kemper, R. Wolski, Phys. Rev. C 64 (2001) 044602.
- [28] E. Browne, Nuclear Data Sheets 99 (2003) 649.
- [29] K. Wildermuth, W. McClure, Springer Tracts in Modern Physics, Vol. 41, edited by G. Höhlen (Springer, New York), 1966.
- [30] G. R. Satchler, Direct Nuclear Reactions, Oxford University Press, New York, 1983, p. 721.
- [31] K. Rusek, I. Martel, J. Gómez-Camacho, A. M. Moro, R. Raabe, Phys. Rev. C 72 (2005) 037603.
- [32] T. Matsumoto, T. Egami, K. Ogata, Y. Iseri, M. Kamimura, M. Yahiro, Phys.Rev. C 73 (2006) 051602.
- [33] A. Moro, K. Rusek, M., J. Arias, J. Gómez-Camacho, M. Rodríguez-Gallardo, Submitted to Phys. Rev. C, arxiv:nuc-th/0703005.
- [34] I. J. Thompson, Comp. Phys. Rep. 7 (1988) 167.

- [35] D. H. Feng, T. Udagawa, T. Tamura, Nucl.Phys. A274 (1976) 262.
- [36] B. F. Bayman, Jongsheng Chen, Phys.Rev. C26 (1982) 1509.
- [37] N. Austern, Y. Iseri, M. Kamimura, M. Kawai, G. Rawitscher, M. Yahiro, Phys. Rep. 154 (1987) 125.
- [38] T. Matsumoto, E. Hiyama, K. Ogata, Y. Iseri, M. Kamimura, S. Chiba, M. Yahiro, Phys.Rev. C 70 (2004) 061601.
- [39] D. G. Kovar, N. Stein, C. K. Bockelman, Nucl.Phys. A231 (1974) 266.
- [40] O. F. Nemets et al., Nucleon clusters in atomic nuclei and many-nucleon transfer reactions (in Russian), Appendix III, Ukrainian Academy of Science, Institute for Nuclear Research, Kiev, 1998.
- [41] Y. F. Smirnov, Y. M. Tchuvil'sky, Phys. Rev. C 15 (1) (1977) 84–93.
- [42] R. L. Varner et al., Phys. Rep. 201 (1991) 57.
- [43] G. Goldring et al., Phys. Lett. B32 (1970) 465.
- [44] J. Bang, C. Gignoux, Nucl. Phys. A313 (1976) 119.
- [45] W. Cárdenas, L. Canto, M. Hussein, Phys. Rev. C 73 (2006) 047603.
- [46] R. Chatterjee, P. Banerjee, R. Shyam, Nucl. Phys. A 692 (2001) 476.